Supporting Information

Tungsten Oxysulphide Nanosheets for Highly Sensitive and Selective NH$_3$ Sensing

Yanan Zheng, [a,§] Lan Sun, [a,§] Weiwei Liu, [a] Chen Wang, [a] Zhengfei Dai, [a,b,]* and Fei Ma [a,]*

[a] State Key Laboratory for Mechanical Behavior of Materials, Xi'an Jiaotong University, Xi'an 710049, Shaanxi, People's Republic of China.

*Corresponding author: mafei@mail.xjtu.edu.cn (F. M.); sensdai@mail.xjtu.edu.cn (Z.D.).

[b] State Key Laboratory for Powder Metallurgy, Central South University, Changsha 410083, China.

[§] These authors contributed equally in this work.

S1. The density functional theory (DFT) calculations

The density functional theory (DFT) calculations were carried in the lattice structures of WS$_2$, tungsten oxysulphide and WO$_3$ to make sure the stable configurations of ammonia molecule absorption. For pure WS$_2$, we considered three absorption sites (Figure S5a-c), namely, on top of a W atom (T$_{W1}$), on top of a S atom (T$_{S1}$), on a hollow

site (T_{h1}). [S1] By comparing the total energy (E_{total}) of the involved sites in Table S3, we choose the stable site T_h with the lowest E_{total}. As for tungsten oxysulphide, in the same way, we choose five absorption sites (Figure S6a-e), on a hollow site (T_{h2}), on top of a O atom with N atom absorbing (T_{O-N}), on top of a S atom (T_{S2}), on top of a W atom (T_{W2}) and on top of a O atom with H atom absorbing (T_{O-H}). The T_{O-H} site of configuration owned the lowest E_{total} (Table S4). For pure WO_3, two sites were considered, on top of a W atom with N atom absorbing (T_{W-N}), on top of a W atom with H atom absorbing (T_{W-H}).[S2] In the process of calculating E_{total} of two sites, T_{W-H} site of configuration is unstable, switching to T_{W-N}, so the E_{total} of T_{W-N} configuration is -312.689 eV (Table S5).
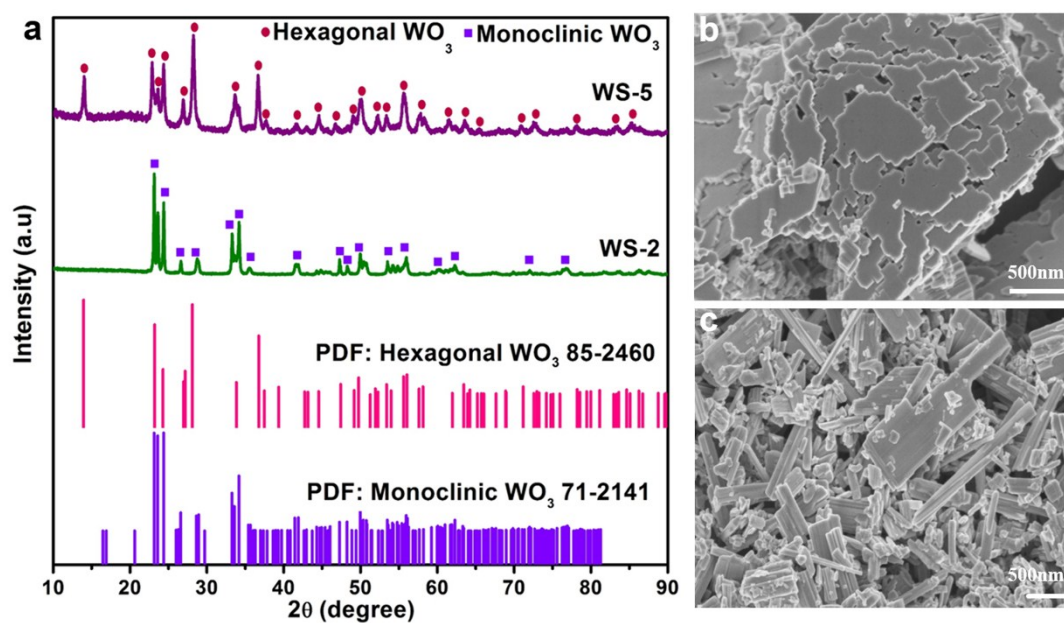
Figure S1. (a) XRD pattern obtained from WS-2 and WS-5 using the different ratios of WCl_6 and TAA (1:2, 1:5). (b, c) Typical SEM image obtained from thin films: (b) hexagonal WO_3 nanosheets, (c) monoclinic WO_3 nanorods.
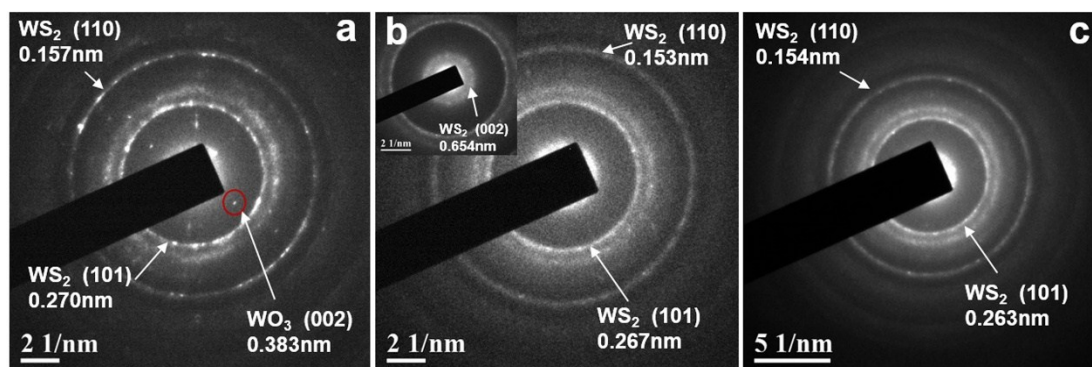
Figure S2. (a) SAED pattern of WS-10. (b) SAED pattern of WS-15. (c) SAED pattern of WS-20.
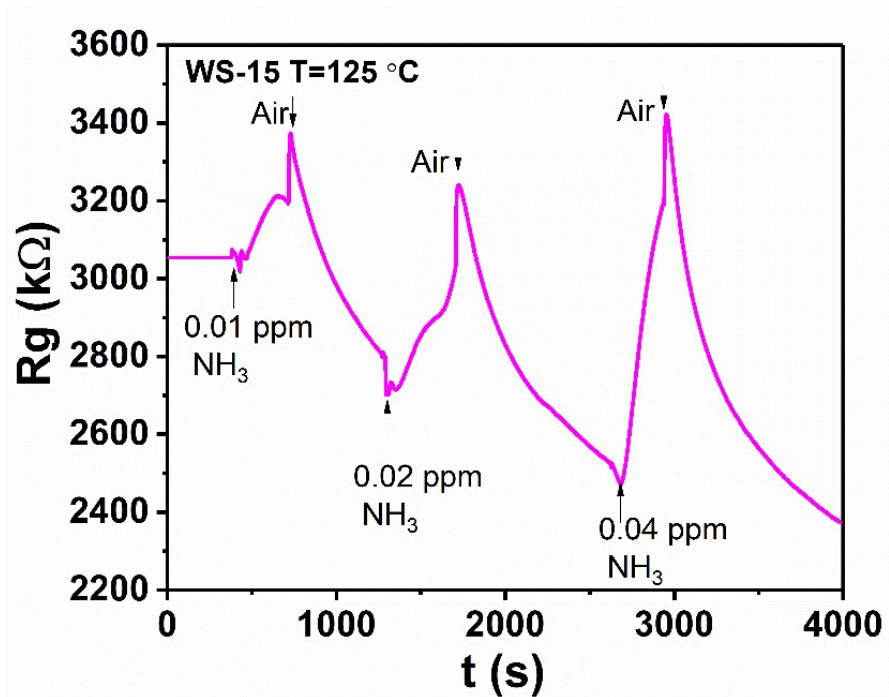
Figure S3. The dynamic sensing signals on exposure to 0.01, 0.02 and 0.04 ppm NH_3 for WS-15 at 125 ºC.
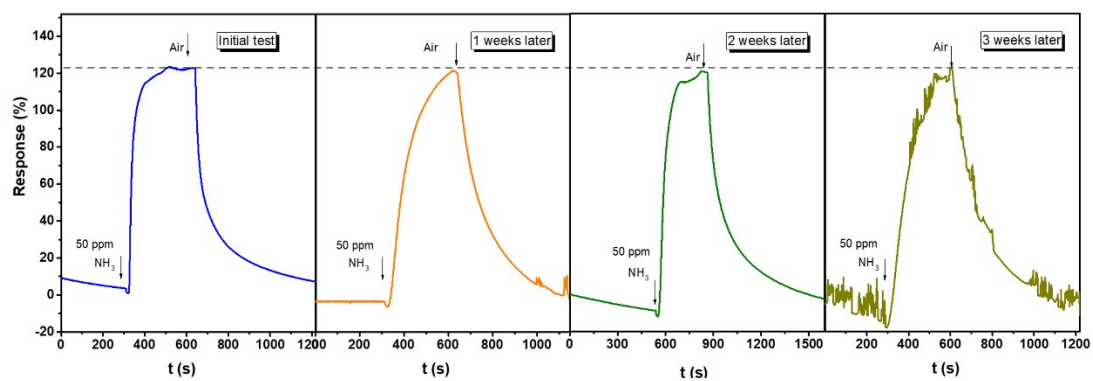
Figure S4. The sensing response of the WS-15 sample toward 50 ppm NH$_3$ at 125 ºC for 3 weeks.
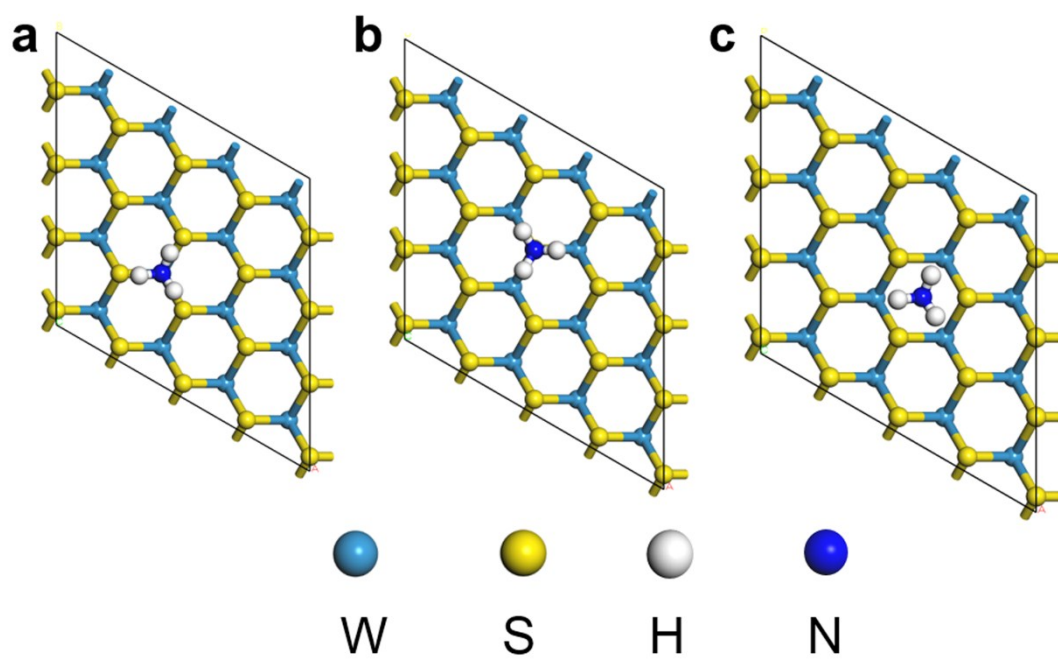
Figure S5. Different sites of WS$_2$ configuration. (a) On top of a W atom (T$_{W1}$). (b) On top of a S atom (T$_{S1}$). (c) On a hollow site (T$_{h1}$).
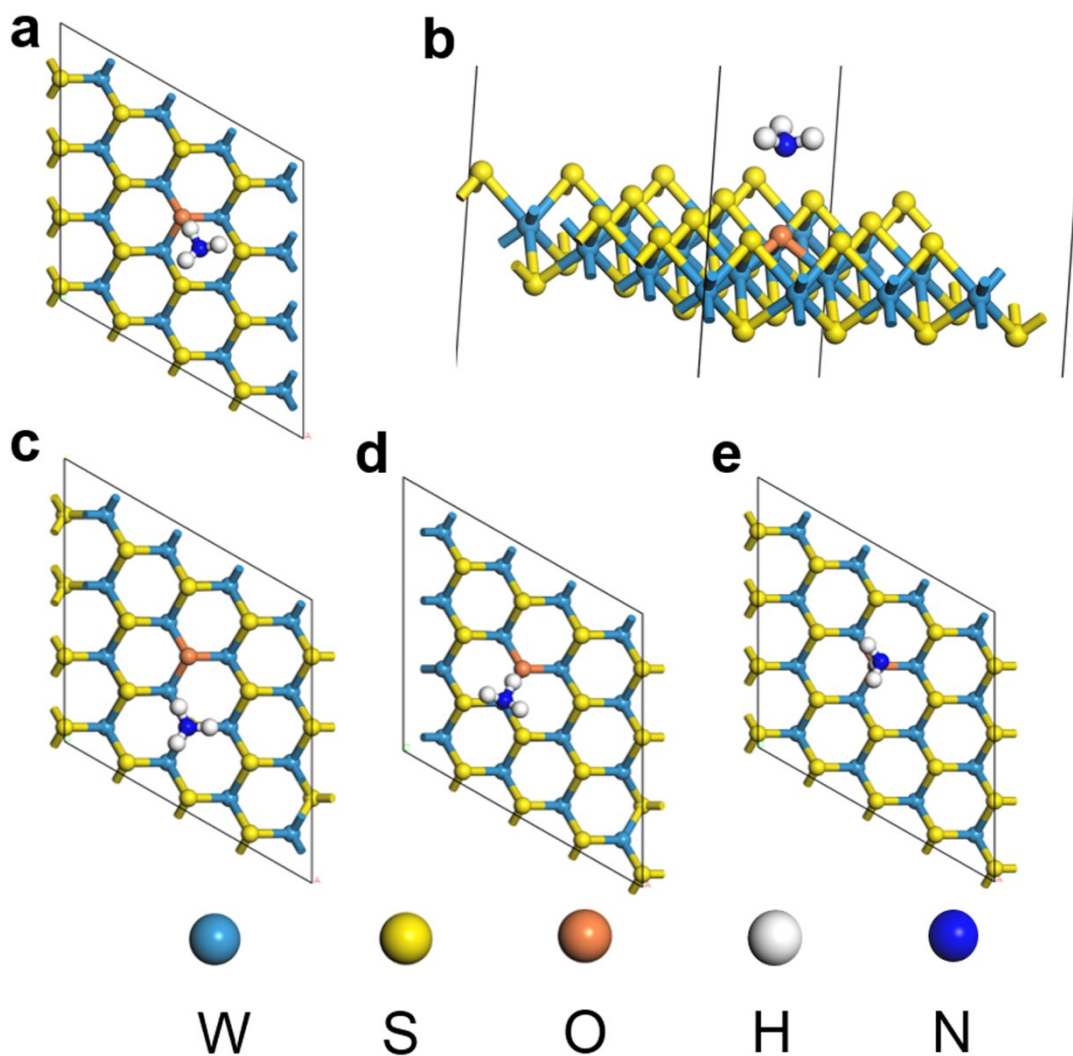
Figure S6. Different sites of tungsten oxysulphide configuration. (a) On a hollow site (T_{h2}). (b) On top of an O atom with N atom absorbing (T_{O-N}). (c) On top of a S atom (T_{S2}). (d) On top of a W atom (T_{W2}). (e) On top of an O atom with H atom absorbing (T_{O-H}).
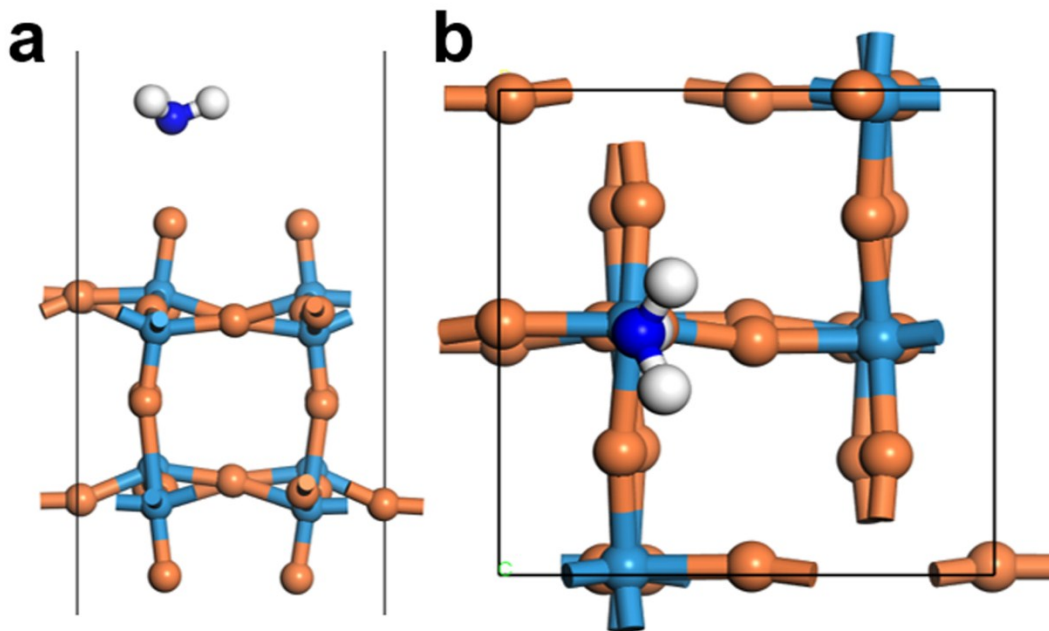
Figure S7. Different sites of WO_3 configuration. (a) On top of a W atom with N atom absorbing (T_{W-N}). (b) On top of a W atom with H atom absorbing (T_{W-H}).
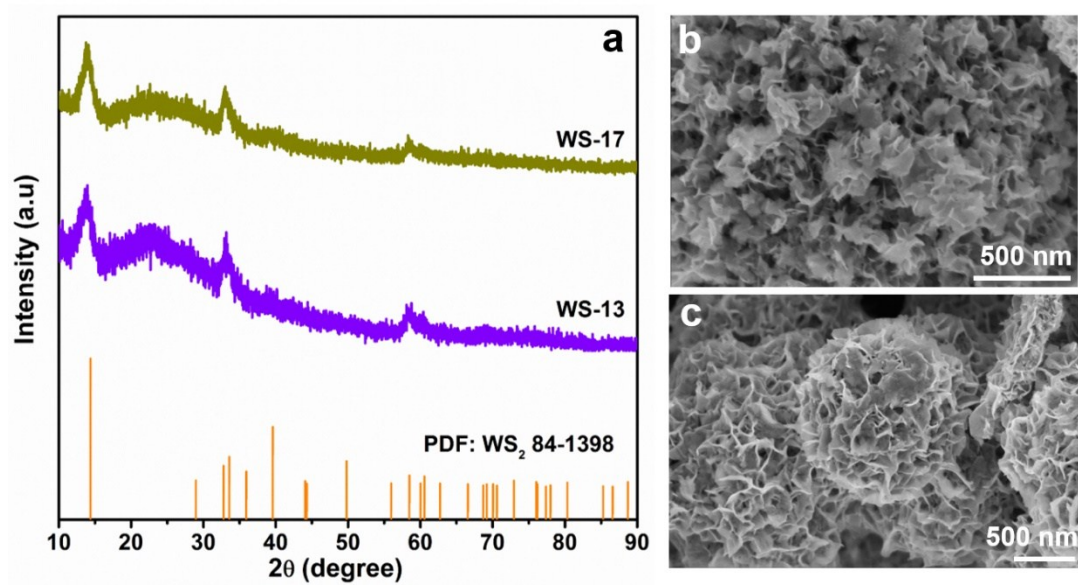
Figure S8. The XRD patterns of WS-13 and WS-17 (a), SEM images of (b) WS-13 and (c) WS-17.
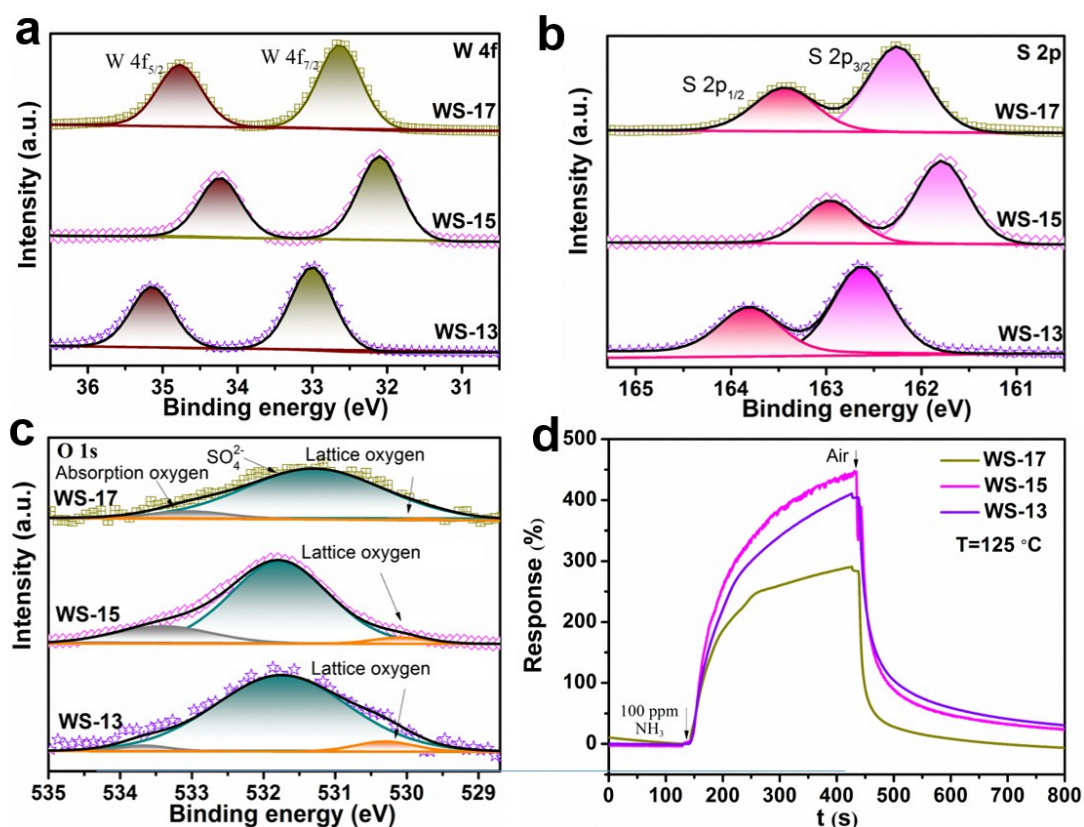
Figure S9. XPS spectra of WS-13, WS-15 and WS-17: (a) W 4f, (b) S2p, (c) O1s, and (d) The sensing responses of WS-13, WS-15 and WS-17 to 100 ppm NH$_3$ at 125 ºC.

As shown in the Figure S8, both the WS-13 and WS-17 samples are featured with the similar phase and nanosheet morphology as the WS-15 materials. The corresponding XPS spectra are presented in t Figure S9a-c, wherein their O/(S+O) molar ratios were calculated as 17.8% (WS-13), 10.9% (WS-15), and 13.7% (WS-15). Figure S9d further compares the sensing properties of WS-13, WS-15 and WS-17 samples to 100 ppm NH$_3$ at 125 ºC.

Table S1. The binding energies of W 4f and S 2p respectively from WS-10, WS-15 and WS-20.

Material	W $4f_{7/2}$ (eV)	W $4f_{5/2}$ (eV)	S $2p_{3/2}$ (eV)	S $2p_{1/2}$ (eV)
WS-10	33.23	35.38	162.87	164.06
WS-15	32.12	34.25	161.79	162.96
WS-20	32.70	34.86	162.40	163.57

Table S2. Comparison of NH_3 sensing performances between tungsten oxysulphide and other reported TMDs.

Sensing material	S (%)	Conc. (ppm)	Lowest Conc. detected (ppm)	Ref.
Single-layer $MoSe_2$	300	300	100	[S3]
SnS_2/SnO_2 composite	148	100	10	[S4]
Au doped MoS_2	120	100	25	[S5]
Exfoliated SnS_2	320	500	20	[S6]
TiO_2 QDs/WS_2	140	500	20	[S7]
PANI-WS_2	81	200	50	[S8]
WS_2/WO_3 nanohybrid	420	1000	250	[S9]
MoS_2 thin film	120	100	10	[S10]
$MoTe_2$	90	100	2	[S11]
Tungsten oxysulphide	450.23	100	0.01	This work

Table S3. The total energies (E_{total}) of WS_2 configuration system at T_{W1}, T_{S1} and T_{h1} sites.

Material	E_{total}-T_{W1} (eV)	E_{total}-T_{S1} (eV)	E_{total}-T_{h1} (eV)
WS_2	-414.03	-413.96	-414.04

Table S4. The total energies (E_{total}) of tungsten oxysulphide configuration system at T_{h2}, T_{O-N}, T_{S2}, T_{W2} and T_{O-H} sites.

Material	Tungsten oxysulphide
E_{total}-T_{h2} (eV)	-415.98
E_{total}-T_{O-N} (eV)	-415.95
E_{total}-T_{S2} (eV)	-415.90
E_{total}-T_{W2} (eV)	-415.95
E_{total}-T_{O-H} (eV)	-416.06

Table S5. The total energies (E_{total}) of WO_3 configuration system at T_{W-N}, and T_{W-H} sites.

Material	E_{total}-T_{W-N} (eV)	E_{total}-T_{W-H} (eV)
WO_3	-312.689	…

Table S6. The $E_{gas/sensors}$, E_{gas}, $E_{sensors}$ and E_a, of tungsten oxysulphide, WS_2 and WO_3.

Material	$E_{gas/sensors}$ (eV)	E_{gas} (eV)	$E_{sensors}$ (eV)	E_a (eV)
WS_2	-414.040	-19.561	-394.306	-0.172
Tungsten oxysulphide	-416.061	-19.561	-396.242	-0.258
WO_3	-312.687	-19.561	-292.956	-0.170

[Reference]

S1 B. Cho, M. G. Hahm, M. Choi, J. Yoon, A. R. Kim, Y. J. Lee, S. G. Park, J. D. Kwon, C. S. Kim, M. Song, Y. Jeong, K. S. Nam, S. Lee, T. J. Yoo, C. G. Kang, B. H. Lee, H. C. Ko, P. M. Ajayan and D. H. Kim, *Scientific Reports*, 2015, **5**, 8052.

S2 Y. Zhang, W. Zeng and Y. Li, *Ceram. Int.*, 2019, **45**, 6043-6050.

S3 D. J. Late, T. Doneux and M. Bougouma, *Appl. Phys. Lett.,* 2014, **105**, 233103

S4 R. Li, K. Jiang, S. Chen, Z. Lou, T. Huang, D. Chen and G. Shen, *RSC Adv.,* 2017, **7**, 52503-52509.

S5 H. Yan, P. Song, S. Zhang, J. Zhang, Z. Yang and Q. Wang, *Ceram. Int*., 2016, **42**, 9327-9331.

S6 Z. Qin, K. Xu, H. Yue, H. Wang, J. Zhang, C. Ouyang, C. Xie and D. Zeng, *Sens. Actuators, B*, 2018, **262**, 771-779.

S7 Z. Qin, C. Ouyang, J. Zhang, L. Wan, S. Wang, C. Xie and D. Zeng, *Sens. Actuators, B*, 2017, **253**, 1034-1042.

S8 R. K. Jha, M. Wan, C. Jacob and P. K. Guha, *New J. Chem*., 2018, **42**, 735-745.

S9 R. K. Jha, C. J. Meher Wan and P. K. Guha, *IEEE Sens. J*., 2018, **18**, 3494-3501.

S10 S. Sharma, A. kumar and D. kaur, *AIP Conf. Proc.,* 2018, **1953**, 030131.

S11 Z. Feng, Y. Xie, J. Chen, Y. Yu, S. Zheng, R. Zhang, Q. Li, X. Chen, C. Sun, H, Zhang, W. Pang, J. Liu and D. Zhang, *2D Mater.,*2017, **4**, 025018.